



# Gravitational Compton scattering at the fourth post-Minkowskian order

Giacomo Brunello<sup>a,b,\*,</sup>, Mario Meo<sup>a,</sup>,<sup>†</sup> and Sid Smith<sup>c,d,e,</sup>,<sup>‡</sup>

<sup>a</sup>*Scuola Normale Superiore, Piazza dei Cavalieri 7, 56126, Pisa, Italy*

<sup>b</sup>*INFN Sezione di Pisa, Largo Pontecorvo 3, 56127 Pisa, Italy*

<sup>c</sup>*Dipartimento di Fisica e Astronomia, Università di Padova, Via Marzolo 8, 35131 Padova, Italy*

<sup>d</sup>*INFN, Sezione di Padova, Via Marzolo 8, I-35131 Padova, Italy. and*

<sup>e</sup>*Higgs Centre for Theoretical Physics, University of Edinburgh, James Clerk Maxwell Building, Peter Guthrie Tait Road, Edinburgh, EH9 3FD, United Kingdom*

(Dated: June 29, 2026)

We compute the classical gravitational Compton amplitude at the fourth post-Minkowskian order,  $\mathcal{O}(G^4)$ , within the Worldline Quantum Field Theory framework. We derive the associated  $N$ -matrix element, which provides the gravitational-wave scattering phase shift at the same order. As a nontrivial check, we show that our result agrees with black-hole perturbation theory.

## I. INTRODUCTION

Precise detection of gravitational-wave (GW) signals requires a deep understanding of the compact objects that generate them. In particular, it is important to characterise the response of compact objects to external perturbations. This response includes conservative tidal deformations, dissipative absorption effects, and more general frequency-dependent effects. For neutron stars, these quantities depend on the equation of state, whereas for black holes, they are fixed predictions of general relativity.

The traditional framework for computing black hole response is black hole perturbation theory (BHPT), which plays a central role in the description of wave propagation in the presence of black holes. For a Schwarzschild black hole, linear gravitational perturbations are governed by the Regge–Wheeler and Zerilli equations [1, 2]. Perturbations of rotating black holes are instead described by the Teukolsky equation [3]. The asymptotic solutions of these wave equations determine partial-wave scattering phase shifts and absorption coefficients. In the low-frequency regime, these quantities can be computed systematically using analytic and numerical methods, including the Mano–Suzuki–Takasugi formalism [4] and related approaches [5]. BHPT therefore provides the general-relativistic answer to wave scattering off a black-hole background.

In parallel, ideas and methods from quantum field theory have led to a new approach to the relativistic two-body problem in general relativity, combining effective field theory (EFT) [6, 7], scattering amplitudes, and worldline methods. These techniques have been predominantly applied across two separate perturbative schemes: The post-Minkowskian expansion for weak-field relativistic scattering between two compact objects and the post-Newtonian expansion for weak-field low-velocity bound

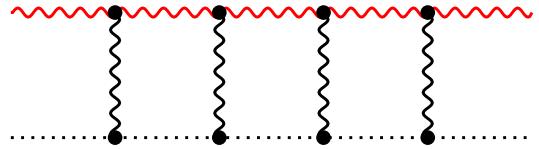


FIG. 1. Three-loop integral topology appearing in the computation of the gravitational Compton amplitude at fourth PM order. Dotted lines represent the compact-object worldline, black wavy lines are potential gravitons, and the red wavy lines are the active retarded graviton propagators.

systems. In the post-Newtonian approach, the combination of EFT ideas [6–8] and multi-loop integration techniques [9] has pushed the study of conservative binary dynamics to 4PN [10, 11] and 5PN orders [12–14], and has recently led to partial results at 6PN [15] and 7PN [16]. In the post-Minkowskian approach, the computation of the 2PM gravitational Hamiltonian from scattering amplitudes [17, 18] initiated a new precision programme for conservative binary dynamics. This programme has since reached 3PM [19–25], 4PM [26–32], and more recently, the 5PM order [33–39]. These results have been obtained using several complementary frameworks for constructing the classical integrand, including scattering-amplitude methods, an observable-based approach [40], worldline quantum field theory (WQFT) [41, 42], and worldline effective field theory [43, 44]. A complementary line of research has focused on radiative observables, using amplitudes and worldline methods to compute gravitational waveforms at leading order [42, 45–51] and, more recently, at next-to-leading order [52–60]. Most of these calculations treat compact objects as point-like sources and therefore do not include finite-size effects.

To incorporate such effects, the compact object must be described by an effective worldline action including non-minimal couplings to the gravitational field. The Wilson coefficients of these operators encode the response of the compact object to external perturbations. Matching these coefficients to BHPT data is therefore a key step toward a systematic description of compact-object

\* [giacomo.brunello@sns.it](mailto:giacomo.brunello@sns.it)

† [mario.meo@sns.it](mailto:mario.meo@sns.it)

‡ [sid.smith@ed.ac.uk](mailto:sid.smith@ed.ac.uk)

response within the EFT framework.

The object that naturally implements this matching is the gravitational Compton amplitude, also known as the gravitational Raman amplitude, which describes the elastic scattering of a gravitational wave off a compact object. In the low-frequency regime, this amplitude admits a post-Minkowskian expansion in powers of  $Gm\omega$ , where  $G$  is Newton's constant,  $m$  is the mass of the compact object, and  $\omega$  is the frequency of the incoming radiation. This quantity has been evaluated at 2PM order [61], including spin effects [62], and recently at 3PM order for a non-spinning compact object [63–65].

In order to match these predictions with BHPT one needs to consider the exponential representation of the scattering matrix [66, 67], and extract the associated  $N$ -matrix, also referred to as the Magnusian operator [68]. This relation has been made explicit for gravitational-wave scattering in Refs. [63–65], where the exponentiated form of the amplitude was matched to the BHPT phase shift.

This perspective has recently played an important role in the study of black-hole Love numbers, dynamical response, and finite-size effects in compact-object scattering [69–72].

Complementarily, the Born-series approach to gravitational amplitudes provides a direct partial-wave framework for matching effective theories to BHPT and for separating long-distance gravitational iterations from short-distance tidal response [72].

In this work, we compute for the first time the minimal spinless gravitational Compton amplitude at fourth post-Minkowskian order in WQFT. The compact object is represented by a worldline coupled to the gravitational field, and classical correlators are generated by Feynman diagrams with retarded boundary conditions ( $+i\epsilon$ ) [41, 42].

For wave scattering, the central object is the graviton two-point function in the presence of the spinless worldline source. We construct the corresponding three-loop WQFT integrand, reduce the resulting tensor structures to scalar integrals, and map the amplitude to a three-loop integral family.

The required integrals are then evaluated using standard multi-loop techniques. We use integration-by-parts identities [73–75] to reduce the amplitude to a basis of 15 master integrals. The master integrals are computed with the method of differential equations [76–80] in the angular variable, and the system is brought to canonical form [81, 82]. The canonical system contains an elliptic sector, and the answer is naturally expressed in terms of elliptic iterated integrals. We check the result by verifying the expected infrared-divergence structure. Finally, we construct the fourth-order  $N$ -matrix operator by subtracting the lower-order Born iterations. We checked our result explicitly by matching it with BHPT.

*Conventions* We work in mostly-minus metric, with signature  $(+, -, -, -)$ . Multi-loop integrals are defined in dimensional regularization:  $D = 4 - 2\epsilon$ , with  $\epsilon$  the analytic regulator. For the loop integration measure we use the

short-hand notation

$$\int_{\ell_1 \dots \ell_L} \equiv \mu^{2\epsilon L} \frac{e^{\epsilon \gamma_E L}}{(4\pi)^{\epsilon L}} \prod_{r=1}^L \int \frac{d^D \ell_r}{(2\pi)^D}. \quad (\text{I.1})$$

Here,  $\mu$  is an arbitrary mass scale coming from dimensional regularization, and  $\gamma_E$  is the Euler–Mascheroni constant.

We denote spatial vectors in boldface, e.g.  $\ell$ , and we use the notation

$$\ell^\mu = (\ell^0, \boldsymbol{\ell}), \quad (\text{I.2})$$

where  $\boldsymbol{\ell}$  is the  $(D-1)$ -dimensional spatial part of the vector  $\ell^\mu$ . With this we also define the short-hand notation

$$\int_{\ell_1 \dots \ell_L} \equiv \mu^{2\epsilon L} \frac{e^{\epsilon \gamma_E L}}{(4\pi)^{\epsilon L}} \prod_{r=1}^L \int \frac{d^{D-1} \ell_r}{(2\pi)^{D-1}}. \quad (\text{I.3})$$

We absorb the factor of  $2\pi$  that appears in the worldline delta functions as

$$\hat{\delta}(y) \equiv 2\pi \delta(y). \quad (\text{I.4})$$

## II. SETTING UP THE PROBLEM

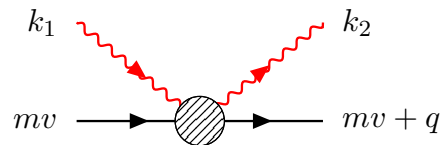


FIG. 2. Kinematics of the problem. The red wavy lines describe the incoming  $k_1$  and outgoing  $k_2$  gravitational wave, while the black line is the worldline of the compact object of mass  $m$  and four-velocity  $v$ . The momentum transfer  $q = k_1 - k_2$ .

We consider the elastic scattering of a gravitational wave off a spinless compact object of mass  $m$ , as depicted in Fig. 2. This process is described by the graviton two-point function in the presence of a single massive worldline source, and is commonly referred to as the gravitational Compton, or gravitational Raman, amplitude.

The compact object is characterised by its gravitational charge  $r_s = Gm$ , while the incoming radiation has wavelength  $\lambda_{\text{rad}} = \omega^{-1}$ , where  $\omega$  is the frequency of the incoming and outgoing radiation. We work in the low-frequency regime

$$Gm\omega \ll 1, \quad r_s \ll \lambda_{\text{rad}}. \quad (\text{II.1})$$

Under these assumptions, the gravitational wave probes only the long-distance field of the compact object. The latter can therefore be described by an effective worldline coupled to gravity. Equivalently, physical observables can be computed in a post-Minkowskian expansion in powers of

$$\epsilon_{\text{PM}} = 2Gm\omega. \quad (\text{II.2})$$

### A. Kinematics

The incoming graviton has momentum  $k_1^\mu$  and helicity  $\lambda_1$ , while the outgoing graviton has momentum  $k_2^\mu$  and helicity  $\lambda_2$ . We define the momentum transfer as

$$q^\mu = k_1^\mu - k_2^\mu. \quad (\text{II.3})$$

The compact object has momentum  $p^\mu = mv^\mu$ , where  $v^\mu$  is the classical four-velocity of the worldline, normalised as  $v^2 = 1$ . The external gravitons are on-shell

$$k_1^2 = k_2^2 = 0. \quad (\text{II.4})$$

Working in the rest frame of the compact object, we have  $v = (1, \mathbf{0})$ . Then elastic scattering implies conservation of the energy measured in the rest frame of the compact object

$$v \cdot k_1 = v \cdot k_2 \equiv \omega, \quad v \cdot q = 0. \quad (\text{II.5})$$

We are also free to parametrize the graviton momenta in terms of the scattering angles in spherical coordinates  $(\theta, \phi)$  as

$$\begin{aligned} k_1 &= \omega(1, 0, 0, 1), \\ k_2 &= \omega(1, \sin\theta \cos\phi, \sin\theta \sin\phi, \cos\theta), \\ q^2 &= -4\omega^2 \sin^2 \frac{\theta}{2} \equiv -4\omega^2 x^2, \end{aligned} \quad (\text{II.6})$$

where we have introduced the dimensionless variable

$$x = \sin \frac{\theta}{2}, \quad 0 \leq x \leq 1. \quad (\text{II.7})$$

Finally, the polarisation tensors are transverse and traceless,

$$k_{i\mu} \varepsilon_{i,\lambda_i}^{\mu\nu} = 0, \quad \eta_{\mu\nu} \varepsilon_{i,\lambda_i}^{\mu\nu} = 0. \quad (\text{II.8})$$

We opt to work in the transverse traceless (TT) gauge, in which the external polarizations are transverse to the worldline velocity

$$v_\mu \varepsilon_{i,\lambda_i}^{\mu\nu} = 0. \quad (\text{II.9})$$

The graviton polarisation tensors can also be rewritten in a double-copy form, as products of spin-1 polarisation vectors as

$$\varepsilon_{i,\lambda_i}^{\mu\nu} = \varepsilon_{i,\lambda_i}^\mu \varepsilon_{i,\lambda_i}^\nu. \quad (\text{II.10})$$

We can parametrise the polarisation vectors in the rest frame as

$$\begin{aligned} \varepsilon_{1,\lambda_1} &= \frac{1}{\sqrt{2}}(0, 1, 0, 0) + \frac{i\lambda_1}{\sqrt{2}}(0, 0, 1, 0), \\ \varepsilon_{2,\lambda_2} &= \frac{1}{\sqrt{2}}(0, \cos\theta \cos\phi, \cos\theta \sin\phi, -\sin\theta) \\ &\quad + \frac{i\lambda_2}{\sqrt{2}}(0, -\sin\phi, \cos\phi, 0). \end{aligned} \quad (\text{II.11})$$

### B. Worldline QFT Setup

The computation is formulated in the worldline quantum field theory (WQFT) framework [41]. The system is described by the action

$$S = S_{\text{EH}} + S_{\text{GF}} + S_{\text{pp}}. \quad (\text{II.12})$$

The bulk dynamics are governed by the Einstein-Hilbert action

$$S_{\text{EH}} = -\frac{2}{\kappa^2} \int d^D x \sqrt{-g} R, \quad (\text{II.13})$$

and we use the de Donder gauge-fixing term

$$S_{\text{GF}} = \frac{1}{\kappa^2} \int d^D x \sqrt{-g} g^{\mu\nu} \Gamma_\mu \Gamma_\nu, \quad (\text{II.14})$$

where  $\Gamma_\mu = g^{\rho\sigma} \Gamma_{\rho\sigma\mu}$  and  $\Gamma_{\rho\sigma\mu}$  are the Christoffel symbols, and  $\kappa^2 = 32\pi G$  is the gravitational coupling constant.

The compact object is described by the gauge-fixed Polyakov form of the massive point-particle action [41]

$$S_{\text{pp}} = -\frac{m}{2} \int d\tau g_{\mu\nu}(x(\tau)) \dot{x}^\mu(\tau) \dot{x}^\nu(\tau). \quad (\text{II.15})$$

Here  $x^\mu(\tau)$  is the worldline position and  $\tau$  is the worldline time parameter. Dots denote differentiation with respect to  $\tau$ . We can study this system perturbatively by expanding the metric around flat spacetime

$$g_{\mu\nu} = \eta_{\mu\nu} + \kappa h_{\mu\nu}, \quad (\text{II.16})$$

and the worldline around the straight trajectory of the compact object

$$x^\mu(\tau) = v^\mu \tau + z^\mu(\tau). \quad (\text{II.17})$$

Here,  $v^\mu$  is the constant asymptotic four-velocity and  $z^\mu(\tau)$  denotes the worldline fluctuation. Substituting these expansions into the action generates the WQFT Feynman rules. The point-particle action produces worldline vertices coupling a single graviton to the compact object, as well as vertices involving the fluctuation field  $z^\mu$ . The Einstein-Hilbert action produces the usual bulk graviton self-interactions. In momentum space, each integration over the straight worldline gives a delta function enforcing the conservation of energy measured along the worldline.

We adopt the causal, or in-in, prescription of WQFT, based on the Schwinger-Keldysh formalism for real-time dynamics [83, 84]. The diagrammatic rules therefore employ retarded propagators, which enforce causal propagation from the worldline source to the radiation field [44, 85]

$$\begin{aligned} \text{wavy line with arrow} &= \frac{i\mathcal{P}_{\mu\nu\rho\sigma}}{(k_0 + i\varepsilon)^2 - \mathbf{k}^2}, \\ \text{straight line with arrow} &= \frac{i\eta_{\mu\nu}}{(k_0 + i\varepsilon)^2 - \mathbf{k}^2}, \end{aligned} \quad (\text{II.18})$$



Loop order $L$	PM order	Diagrams
0	1PM	2 (1)
1	2PM	6 (3)
2	3PM	20 (10)
3	4PM	70 (36)

TABLE I. WQFT diagrams generated by the recursion (III.12) at loop order  $L$ , corresponding to PM order  $n = L + 1$ . The numbers in parentheses denote the diagrams that survive after imposing  $v_\mu \varepsilon_i^{\mu\nu} = 0$ .

The Kronecker delta in Eq. (III.8) reflects that recoil enters only as this leading insertion; higher-order recoil diagrams arise by iterating it together with the background kernels inside the recursion, not from new kernels.

Expanding the kernel and the connected two-point function perturbatively as

$$\mathcal{K} = \sum_{r \geq 1} \mathcal{K}^{(r)}, \quad \mathcal{G} = \sum_{n \geq 0} \mathcal{G}^{(n)}, \quad \mathcal{G}^{(0)} = \mathcal{G}_0, \quad (\text{III.11})$$

the recursion (III.7) with the kernel split (III.8) becomes

$$\begin{aligned} \mathcal{G}^{(n)} &= \sum_{r=1}^n \mathcal{K}_{\text{bg}}^{(r)} \mathcal{G}^{(n-r)} \\ &+ \mathcal{K}_{\text{rec}} \mathcal{G}^{(n-1)}, \end{aligned} \quad (\text{III.12})$$

which generates all connected WQFT diagrams with one incoming and one outgoing active graviton.

The diagrams generated by Eq. (III.12) have a simple causal structure. Potential gravitons, which carry vanishing energy in the rest frame of the compact object, build the static field  $H_{\mu\nu}$ , while active gravitons carry the external frequency  $\omega$  and propagate the gravitational wave through this field. With retarded boundary conditions, causality flows from the incoming to the outgoing active graviton, and only active lines can go on shell.

Each worldline insertion produces a delta function  $\hat{\delta}(v \cdot Q)$ , with  $Q^\mu$  the total momentum entering the worldline segment, while bulk vertices impose ordinary  $D$ -dimensional momentum conservation. These constraints fix the energy flow along the worldline, so that the  $n$ PM contribution is an  $(n-1)$ -loop spatial integral.

The recursion generates 70 WQFT diagrams at 4PM order, of which only 36 contribute after imposing the external-polarisation gauge of Eq. (II.9). The diagram counts through 4PM order are collected in Tab. I. The Wick contractions, index contractions, and tensor simplifications needed to construct the momentum-space integrands were carried out with an in-house FORM [88] implementation, using the on-shell conditions, the transversality and tracelessness of the external gravitons, the elastic relation  $v \cdot q = 0$ , and the kinematic identities of Sec. II. As checks, we verified the external Ward identities and reproduced the lower-order WQFT results of Refs. [63–65].

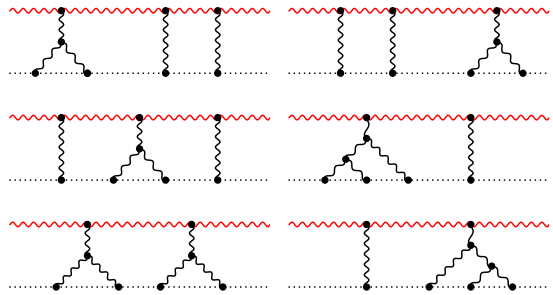


FIG. 3. Reducible top sectors appearing in the three-loop Compton amplitude.

## B. Integral reduction

The recursive construction gives a sum of diagrammatic integrands with different momentum routings and worldline delta functions. The integrand is characterised by tensor integrals up to rank 4, where tensors contain polarisation vectors contracted with loop momenta  $\varepsilon_i \cdot \ell_j$ .

The tensors are reduced to scalar integrals using an in-house implementation of the Passarino-Veltman reduction in FORM, as described in Ref. [89]. All tensor dependence can be expressed in terms of three independent gauge-invariant structures [61]

$$\begin{aligned} \mathcal{T}_1 &\equiv (v \cdot F_1 \cdot F_2^* \cdot v)^2, \\ \mathcal{T}_2 &\equiv (F_1 \cdot F_2^*)(v \cdot F_1 \cdot F_2^* \cdot v), \\ \mathcal{T}_3 &\equiv (F_1 \cdot F_2^*)^2, \end{aligned} \quad (\text{III.13})$$

where  $F_i^{\mu\nu} = k_i^\mu \varepsilon_i^\nu - k_i^\nu \varepsilon_i^\mu$  is the linearised field strength of the external graviton. In this basis, the integrand can be written as a linear combination of the three tensor structures  $\mathcal{T}_i$ . We map the resulting scalar integrals for all diagrams to a single class of integrals by employing an in-house topology-mapping algorithm in FORM that performs shifts of loop momenta to identify graphs by exploiting the structure of their associated Symanzik polynomials. The resulting integral family is given by

$$F_{n_1 \dots n_{12}} = \int_{\ell_1 \ell_2 \ell_3} \frac{\prod_{r=1}^3 \hat{\delta}(v \cdot \ell_r)}{\prod_{a=1}^{12} D_a^{n_a}}, \quad (\text{III.14})$$

where the propagators are

$$\begin{aligned} D_a &= (\ell_a^0 + k_1^0 + i\varepsilon)^2 - (\ell_a + \mathbf{k}_1)^2, \\ D_{3+a} &= \ell_a^2, \\ D_{6+a} &= (\ell_a + q)^2, \\ D_{9+a} &= (\ell_{a+1} - \ell_a)^2, \quad \ell_4 = \ell_1, \end{aligned} \quad (\text{III.15})$$

where  $a = 1, 2, 3$ . These integrals depend on two kinematic variables: the graviton frequency  $\omega = v \cdot k_i$  and the angular variable  $x$ . There are 7 highest-level sectors

appearing with 7 denominators, of which only one is irreducible, shown in Fig. 1; the reducible ones are shown in Fig. 3.

We perform integration-by-parts (IBP) reduction using the code PRISM [90], based on syzygy-based methods [91–94], improved seeding algorithms [92, 93, 95], and finite-field reconstruction techniques as implemented in FiniteFlow [96].

After IBP reduction, the amplitude can be expressed in terms of a basis of 15 master integrals, spanning over 10 sub-topologies, depicted in Fig. 4, which are all sub-sectors of the irreducible top sector in Fig. 1. The number of master integrals for each sub-topology is given by the following set of integrals:

$$\mathcal{G}_{1,\dots,6} : 1, \quad \mathcal{G}_{7,8,9} : 2, \quad \mathcal{G}_{10} : 3. \quad (\text{III.16})$$

Interestingly, we find that 7 of the 36 diagrams are zero after IBP reduction. These 7 diagrams are the only ones containing a worldline propagator. We observed the same pattern at lower loops and therefore conjecture that this holds at all orders in the TT gauge.

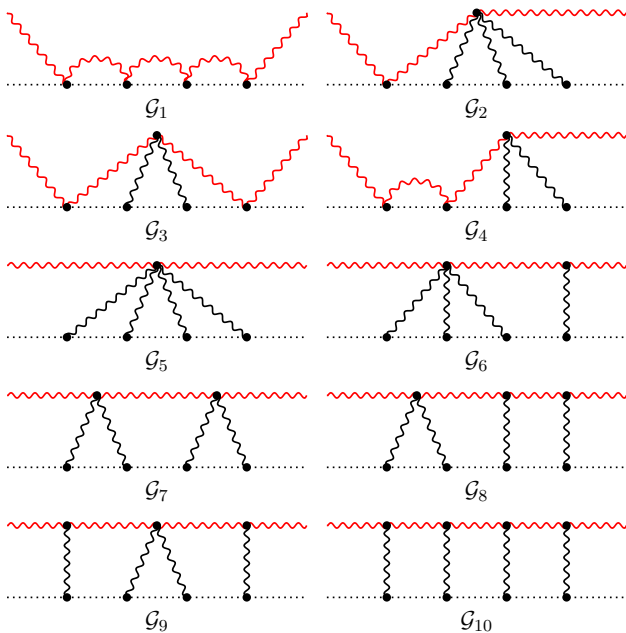


FIG. 4. 10 master integral topologies  $\{\mathcal{G}_i\}_{i=1}^{10}$  containing the 15 master integrals appearing in the three-loop integral reduction. The red wavy lines represent the retarded graviton propagators (see Sec. III C), while black wavy lines represent the potential graviton propagators. Black dotted lines denote worldline delta functions.

### C. Integral evaluation

In order to evaluate the master integrals, we solve the associated differential equations that the master integrals obey and fix the boundary conditions in the forward-scattering limit.

We first note that all propagators come with a retarded prescription, as dictated by the Feynman rules; however, due to the worldline delta functions, this only has an effect on propagators  $D_{1,2,3}$ . Therefore, we refer to these as the *retarded propagators* ( $+i\varepsilon$ ). This can be seen by imposing the delta functions, after which the family takes the form

$$F_{n_1\dots n_{12}}^{(\eta_1\eta_2\eta_3)} = \int_{\ell_1\ell_2\ell_3} \frac{1}{\prod_{a=1}^3 \tilde{D}_a(\eta_a)^{n_a} \prod_{a=4}^{12} \tilde{D}_a^{n_a}}, \quad (\text{III.17})$$

where

$$\begin{aligned} \tilde{D}_a &= (\omega + i\eta_a\varepsilon)^2 - (\ell_a + \mathbf{k}_1)^2, \\ \tilde{D}_{3+a} &= -\ell_a^2, \\ \tilde{D}_{6+a} &= -(\ell_a + \mathbf{q})^2, \\ \tilde{D}_{9+a} &= -(\ell_{a+1} - \ell_a)^2, \quad \ell_4 = \ell_1. \end{aligned} \quad (\text{III.18})$$

In order to eventually calculate the phase shift associated to the scattering amplitude, we will need the integrals evaluated with *advanced propagators* ( $-i\varepsilon$ ) as well, this is why we have included the prescriptions  $\eta_a = \pm$ . The resulting irreducible top sector after imposing the delta function is depicted in Fig. 5.

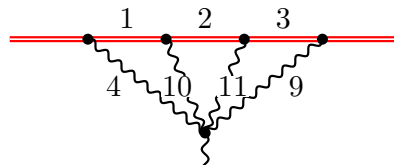


FIG. 5. Three-loop master integral topology after imposing the worldline delta functions. The red double lines represent massive propagators with mass  $\omega$ , while black wavy lines represent massless propagators.

### Differential Equations

We denote the set of master integrals by  $\mathbf{J}$ , and these satisfy a system of differential equations in the kinematic variable  $x$ <sup>1</sup>

$$\partial_x \mathbf{J}(x, \epsilon) = A(x, \epsilon) \mathbf{J}(x, \epsilon). \quad (\text{III.19})$$

A convenient choice of  $\mathbf{J}$  is the canonical basis [81], where the dependence on the spacetime dimension parameter  $\epsilon$  is factorised from the kinematic dependence.

$$\partial_x \mathbf{J}(x, \epsilon) = \epsilon \hat{A}(x) \mathbf{J}(x, \epsilon). \quad (\text{III.20})$$

To find the canonical basis, we used a combination of methods involving leading singularities [97–100], Magnus

<sup>1</sup> The dependence of the integrals on the graviton frequency  $\omega$  is trivially found by dimensional analysis.

expansion [82], and the publicly available code CANONICA [101]. The explicit form of the canonical differential equation is reported in the ancillary file `de_canonical.m`.

The system is characterised by a family of elliptic integrals that appears in the sector  $\mathcal{G}_7$  of Fig. 4, which is the solution of the following second-order differential operator:

$$\left( \partial_x^2 - \frac{3x^2 - 1}{x(1-x^2)} \partial_x - \frac{1}{1-x^2} \right) w_0 = 0. \quad (\text{III.21})$$

In the kinematic region  $0 \leq x \leq 1$ , this is given by the first elliptic period

$$w_0(x) = \frac{2}{\pi} K(x^2). \quad (\text{III.22})$$

Details on the canonical differential equation system are given in App. A. The solution can be expressed in terms of iterated integrals [102, 103], which, in this case, are given by elliptic polylogarithms [104, 105]

$$\mathbf{J} = \left( \mathbf{1} + \epsilon \int_0^x dx' \hat{A}(x') + \epsilon^2 \int_0^x dx' \hat{A}(x') \int_0^{x'} dx'' \hat{A}(x'') + \dots \right) \mathbf{J}_b, \quad (\text{III.23})$$

where  $\mathbf{J}_b$  is a boundary vector at the kinematic point  $x = 0$ . The integration kernel consists of the logarithmic singularities  $(x, x+1, x-1)$  and the elliptic periods  $w_0, w'_0$ .

Boundary conditions

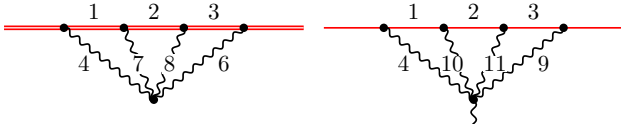


FIG. 6. Boundary integral topologies in the hard (left) and soft (right) regions. In the hard region this is a three-loop two-point function with three massive propagators (red double lines). In the soft region we have a three-loop three-point function with three eikonal propagators (red single lines).

For the boundary conditions, we analyse the behaviour of the master integrals in the forward-scattering limit

$$x \rightarrow 0. \quad (\text{III.24})$$

In this limit, the differential equations develop a regular singular point, and the asymptotic behaviour of the master integrals can be studied using the method of regions [106–108]. At three loops, there are two relevant regions that correspond to the scaling of the loop momenta as

$$\text{hard region: } \ell_i \sim \omega, \quad \text{soft region: } \ell_i \sim \omega x.$$

To minimise the number of integrals to compute, we study the asymptotic regions at the level of the differential equations [51, 109–111]. Such a strategy has already been studied in the two-loop case in Refs. [64, 65]. The possible regions contributing are dictated by the eigenvalues of the residue matrix of the system at  $x = 0$

$$\epsilon \hat{A}(x, \epsilon) \stackrel{x \rightarrow 0}{=} \epsilon \frac{\hat{A}_0(\epsilon)}{x} + \mathcal{O}(x^0). \quad (\text{III.25})$$

In particular, at three loops, we can perform a Jordan decomposition of the residue matrix, finding 3 regions

$$M \cdot \epsilon \hat{A}_0 \cdot M^{-1} = \text{Diag}[0^{\times 6}, (-6\epsilon)^{\times 6}, (2\epsilon)^{\times 3}], \quad (\text{III.26})$$

Here, the eigenvalue 0 corresponds to the hard region, and the  $(-6\epsilon)$  corresponds to the soft region. The eigenvalue  $(2\epsilon)$  represents a spurious region, and we need to impose that the integral vanishes in that region. Hence, the generic boundary vector is given by

$$\mathbf{J}_b = \mathbf{J}_0 + x^{-6\epsilon} \mathbf{J}_{-6\epsilon}. \quad (\text{III.27})$$

where  $\mathbf{J}_0$  and  $\mathbf{J}_{-6\epsilon}$  are the boundary vectors for the hard and soft regions, respectively. The new basis of master integrals  $\mathbf{J}' = M \cdot \mathbf{J}$  diagonalizes the asymptotic behaviour of the system at  $x = 0$ . For the two regions, we perform an expansion under the integral sign, leading to two distinct families of integrals, depicted in Fig. 6.

*a. Hard region.* In the hard region, the integral family becomes a three-loop two-point function with three massive propagators:

$$F_{n_1 \dots n_9}^h(\eta_1, \eta_2, \eta_3) = \int_{\ell_1 \ell_2 \ell_3} \frac{1}{\prod_{a=1}^9 (\tilde{D}_a^h)^{n_a}}, \quad (\text{III.28})$$

where

$$\begin{aligned} \tilde{D}_a^h(\eta_a) &= (\ell_a + \mathbf{k}_1)^2 - (\omega + i\eta_a \varepsilon)^2, \\ \tilde{D}_{3+a}^h &= \ell_a^2, \\ \tilde{D}_{6+a}^h &= (\ell_{a+1} - \ell_a)^2, \quad \ell_4 = \ell_1. \end{aligned} \quad (\text{III.29})$$

Using IBPs, we find 6 master integrals appearing

$$\begin{aligned} F_{111000000}^h, & \quad F_{100001110}^h, & \quad F_{101000110}^h, \\ F_{110001010}^h, & \quad F_{010101110}^h, & \quad F_{111101110}^h. \end{aligned} \quad (\text{III.30})$$

Such MIs have already appeared in the context of  $g-2$  computations (see, e.g., [112, 113]).

*b. Soft region.* In the soft region, the integral family is that of a soft three-loop triangle with eikonal propagators

$$F_{n_1 \dots n_{12}}^s(\eta_1, \eta_2, \eta_3) = \int_{\ell_1 \ell_2 \ell_3} \frac{1}{\prod_{a=1}^{12} (\tilde{D}_a^s)^{n_a}}, \quad (\text{III.31})$$

where

$$\tilde{D}_a^s(\eta_a) = \ell_a \cdot \mathbf{k}_1 - i\eta_a \varepsilon,$$

$$\begin{aligned}
\tilde{D}_{3+a}^s &= \ell_a^2, \\
\tilde{D}_{6+a}^s &= (\ell_a + \mathbf{q})^2, \\
\tilde{D}_{9+a}^s &= (\ell_{a+1} - \ell_a)^2, \quad \ell_4 = \ell_1.
\end{aligned} \tag{III.32}$$

Using IBPs, we find 6 master integrals appearing

$$\begin{aligned}
F_{0001000011110}^s(\eta_1, \eta_2, \eta_3), & \quad F_{0011000011110}^s(\eta_1, \eta_2, \eta_3), & \quad F_{0101000011110}^s(\eta_1, \eta_2, \eta_3), \\
F_{0111000011110}^s(\eta_1, \eta_2, \eta_3), & \quad F_{1011000011110}^s(\eta_1, \eta_2, \eta_3), & \quad F_{1111000011110}^s(\eta_1, \eta_2, \eta_3).
\end{aligned} \tag{III.33}$$

Integrals of this type typically appear in the context of HQET (see, e.g., [114]). Their analytic expressions have already been computed in Refs. [115, 116].

Boundary integrals do not depend on any kinematic scale; for this reason, it is very convenient to evaluate them using numerical methods. For this task, we used AMFLOW [117] to compute all boundary integrals numerically up to at least 200 digits of precision. The analytic expressions were then reconstructed with a suitable choice of transcendental functions using the PSLQ algorithm implemented within POLYLOGTOOLS [105].

We checked against known results in both regions. We also computed many of the integrals via Mellin-Barnes and direct integration techniques. Further details and analytic results are reported in Appendix B. The ancillary file `retarded_boundary.m` contains the boundary integrals for the canonical basis up to  $\mathcal{O}(\epsilon^0)$  in the fully retarded case ( $\eta_i = +$ ).

#### IV. RESULT

The amplitude at all orders takes the following form

$$i\mathcal{M}(\lambda_1, \lambda_2) = \sum_{n=1}^{\infty} \sum_{k=1-n}^{\infty} \epsilon^k i\mathcal{M}_k^{(n)}(\lambda_1, \lambda_2), \tag{IV.1}$$

and contains infrared divergences as predicted by Weinberg [118–120].

We note that tree level has no  $\epsilon$ -dependence, and so  $\mathcal{M}_{k>0}^{(1)} = 0$ . Infrared divergences exponentiate, and we can define the finite part of the amplitude as

$$i\mathcal{M}_{\text{fin}}(\lambda_1, \lambda_2) = e^{i\epsilon_{\text{PM}}/\epsilon} i\mathcal{M}(\lambda_1, \lambda_2). \tag{IV.2}$$

This finite part relates to the scattering cross-section and can be used to match with BHPT following the procedure outlined in Ref. [63]. The divergent part at all orders has the following structure

$$\mathcal{M}_{-k}^{(n)} = (-1)^k \sum_{m=1}^{n-k} \frac{(i\epsilon_{\text{PM}})^{n-m} \binom{n-m-1}{k-1}}{(n-m)!} \mathcal{M}_{n-k-m}^{(m)}, \tag{IV.3}$$

for  $k > 0$ , which we have verified for  $n \leq 4$ . At fourth post-Minkowskian order, we have the structure

$$i\mathcal{M}^{(4)} = \frac{i\mathcal{M}_{-3}^{(4)}}{\epsilon^3} + \frac{i\mathcal{M}_{-2}^{(4)}}{\epsilon^2} + \frac{i\mathcal{M}_{-1}^{(4)}}{\epsilon} + i\mathcal{M}_0^{(4)}$$

$$\begin{aligned}
&= -\frac{\epsilon_{\text{PM}}^3 \mathcal{M}_0^{(1)}}{6\epsilon^3} - \frac{i\epsilon_{\text{PM}}^2 \mathcal{M}_0^{(2)}}{2\epsilon^2} \\
&+ \frac{1}{\epsilon} \left( \frac{i\epsilon_{\text{PM}}^2}{2} \mathcal{M}_1^{(2)} + \epsilon_{\text{PM}} \mathcal{M}_0^{(3)} \right) + i\mathcal{M}_0^{(4)}.
\end{aligned} \tag{IV.4}$$

The contributions  $i\mathcal{M}_k^{(4)}$  are provided in the ancillary file `iM_4pm.m`.

#### A. Extracting the phase shift

To connect the 4PM scattering amplitude of Eq. (IV.4) with BHPT, we need to consider the exponential representation of the scattering matrix [66, 68, 121]

$$\hat{S} = e^{i\hat{N}}. \tag{IV.5}$$

As shown in Refs. [64, 65], the matrix elements of  $\hat{N}$

$$\langle k_2, \lambda_2 | i\hat{N}^{(n)} | k_1, \lambda_1 \rangle = \hat{\delta}(v \cdot \mathbf{q}) i\mathcal{N}_{\lambda_1 \lambda_2}^{(n)}(x, \phi). \tag{IV.6}$$

are the objects that map directly onto the partial-wave phase shift. They are obtained from the transfer matrix by expanding

$$i\hat{N} = \log(1 + i\hat{T}). \tag{IV.7}$$

Both operators admit a PM expansion

$$i\hat{T} = \sum_{n \geq 1} i\hat{T}^{(n)}, \quad i\hat{N} = \sum_{n \geq 1} i\hat{N}^{(n)}. \tag{IV.8}$$

Inserting these expansions into the operator formula, we get

$$\begin{aligned}
i\hat{N}^{(4)} &= i\hat{T}^{(4)} \\
&- \frac{1}{2} (i\hat{T}^{(1)} \cdot i\hat{T}^{(3)} + i\hat{T}^{(2)} \cdot i\hat{T}^{(2)} + i\hat{T}^{(3)} \cdot i\hat{T}^{(1)}) \\
&+ \frac{1}{3} (i\hat{T}^{(1)} \cdot i\hat{T}^{(1)} \cdot i\hat{T}^{(2)} + i\hat{T}^{(1)} \cdot i\hat{T}^{(2)} \cdot i\hat{T}^{(1)} \\
&+ i\hat{T}^{(2)} \cdot i\hat{T}^{(1)} \cdot i\hat{T}^{(1)}) \\
&- \frac{1}{4} i\hat{T}^{(1)} \cdot i\hat{T}^{(1)} \cdot i\hat{T}^{(1)} \cdot i\hat{T}^{(1)}.
\end{aligned} \tag{IV.9}$$

Enforcing unitarity perturbatively as done in Ref. [65]

$$T - T^\dagger = iTT^\dagger, \tag{IV.10}$$

we obtain at 4PM

$$\begin{aligned}
i\hat{N}^{(4)} &= \text{Im} [i\hat{T}^{(4)}] + \frac{1}{4} i\hat{T}^{(1)} \cdot i\hat{T}^{(1)} \cdot i\hat{T}^{(1)} \cdot i\hat{T}^{(1)} \\
&- \frac{1}{6} (i\hat{T}^{(2)} \cdot i\hat{T}^{(1)} \cdot i\hat{T}^{(1)} + i\hat{T}^{(1)} \cdot i\hat{T}^{(2)} \cdot i\hat{T}^{(1)} \\
&+ i\hat{T}^{(1)} \cdot i\hat{T}^{(1)} \cdot i\hat{T}^{(2)}),
\end{aligned} \tag{IV.11}$$

where with  $\cdot$  we denote the insertion of a complete set of intermediate on-shell graviton states

$$(X_1 \cdot X_2)_{fi} = \int_{\lambda, \ell} \hat{\delta}_+(\ell^2) \langle f | \hat{X}_1 | \ell, \lambda \rangle \langle \ell, \lambda | \hat{X}_2 | i \rangle, \tag{IV.12}$$

and for products with more factors, we have analogous multiple phase-space integrals. The subtraction terms in Eq. (IV.11) correspond to unitarity cuts of scattering amplitudes. Considering the propagator labelling of Eq. (III.15), we have for the matrix element  $\mathcal{N}^{(4)}$

$$\begin{aligned} i\mathcal{N}^{(4)} &= \text{Im} [i\mathcal{M}^{(4)}] - \frac{i}{4} \text{Cut}_{(123)} [i\mathcal{M}^{(4)}] \\ &+ \frac{1}{6} (\text{Cut}_{(12)} [i\mathcal{M}^{(4)}] + \text{Cut}_{(13)} [i\mathcal{M}^{(4)}] \\ &+ \text{Cut}_{(23)} [i\mathcal{M}^{(4)}]). \end{aligned} \quad (\text{IV.13})$$

The various cuts of the 3-loop scattering amplitudes  $\text{Cut}_{(\dots)} [i\mathcal{M}^{(4)}]$  are obtained by simply applying the associated cut at the level of the master integrals and substituting the corresponding cut propagators with on-shell delta functions normalised as  $(2\pi i)\delta(D)$ . Hence, the matrix element  $i\mathcal{N}^{(4)}$  can be obtained by considering cut-subtracted master integrals

$$\tilde{J}_i = \text{Re}[J_i] - \frac{i}{4} \text{Cut}_{(123)}[J_i]$$

---


$$\begin{aligned} \mathcal{N}_{++}^{(4)}(x, \phi) &= \frac{\epsilon_{PM}^4 \pi^2 e^{2i\phi}}{\omega(1-x^2)} \left[ 4(7+11x^2) \log(1+x) + \frac{2xp_1(x)w'_0(x) + p_2(x)w_0(x)}{1536} \left( \frac{\pi^2}{4} - \mathcal{G}_1(x) + \frac{w_1(x)}{w_0(x)} \mathcal{G}_0(x) \right) \right. \\ &\quad \left. - \frac{1}{1-x^2} \left( \frac{4}{3} \pi^2 p_3(x) + \frac{(1-x)p_4(x)}{23040} + 16p_3(x)\text{Li}_2(-x) + \frac{p_1(x)}{768} \frac{\mathcal{G}_0(x)}{w_0(x)} \right) \right], \\ \mathcal{N}_{+-}^{(4)}(x, \phi) &= 0. \end{aligned} \quad (\text{IV.16})$$

where

$$\begin{aligned} \mathcal{G}_i(x) &= \int_0^x dx' w_i(x'), \quad i=0,1, \\ p_1(x) &= 17805x^4 + 113738x^2 + 44273, \\ p_2(x) &= 25485x^4 + 120355x^2 + 29976, \\ p_3(x) &= 2x^4 + 6x^2 + 1, \\ p_4(x) &= 1575x^6 + 47655x^5 + 827547x^4 + 366747x^3, \\ &\quad + 3142262x^2 + 166262x + 722432, \end{aligned} \quad (\text{IV.17})$$

and  $w_i(x)$  are the elliptic periods

$$w_0(x) = \frac{2}{\pi} K(x^2), \quad w_1(x) = K(1-x^2). \quad (\text{IV.18})$$

We notice that the result is finite and is expressed in terms of a small set of functions:

$$\{\log(1+x), \text{Li}_2(-x), w_i(x), \mathcal{G}_i(x)\}. \quad (\text{IV.19})$$

Eq. (IV.16) is also reported in the ancillary file `N_matrix_4pm.m`. We remark that no explicit computation of cuts of scattering amplitudes was needed.

$$+ \frac{1}{6} (\text{Cut}_{(12)} + \text{Cut}_{(13)} + \text{Cut}_{(23)}) [J_i]. \quad (\text{IV.14})$$

Furthermore, since the analytic dependence of the integrals on  $x$  is invariant under cuts, it is sufficient to consider only cut-subtracted boundary conditions. These have been computed numerically using `AMFLOW`, and via reverse-unitarity [122, 123], rewriting delta functions as a linear combination of advanced and retarded propagators

$$(2\pi i)\delta(p^2) = \frac{1}{(p^2 - i\varepsilon)} - \frac{1}{(p^2 + i\varepsilon)}. \quad (\text{IV.15})$$

The explicit result for the cut-subtracted boundary vectors in the canonical basis that directly give the phase shift is available in the ancillary file `iterated_boundary.m`. The 4PM matrix elements for the helicity-conserving ( $\lambda_1 = \lambda_2$ ) and helicity-reversing ( $\lambda_1 = -\lambda_2$ ) cases are surprisingly simple and read as

---

## B. Matching with BHPT

To match the matrix element of Eq. (IV.16) with BHPT, we followed the approach outlined in Ref. [64]. The BHPT computation is naturally formulated in a basis of spin-weighted spherical harmonics. For a Schwarzschild background, the two parity sectors are described by the Regge–Wheeler and Zerilli radial equations. The large-radius solution defines the partial-wave scattering matrix

$${}_{-2}S_{\ell 2}^P = {}_{-2}\eta_{\ell 2} e^{2i-2\delta_{\ell 2}^P}, \quad P = \pm 1, \quad (\text{IV.20})$$

where  $P$  labels the even and odd parity channels. In the low-frequency expansion, the absorption factor starts beyond the order considered in this paper,  ${}_{-2}\eta_{\ell 2} = 1 + \mathcal{O}(\varepsilon_{\text{PM}}^5)$ . Thus, the conservative information through 4PM is fully contained in the real phase shifts

$${}_{-2}\delta_{\ell 2}^P = \sum_{n \geq 1} \varepsilon_{\text{PM}}^n {}_{-2}\delta_{\ell 2}^{P,(n)}. \quad (\text{IV.21})$$

From the matrix element  $\mathcal{N}_{\lambda_1 \lambda_2}^{(n)}(x, \phi)$ , we define the helicity-preserving and helicity-reversing partial-wave

modes from the matrix element  $\mathcal{N}_{\lambda_1\lambda_2}^{(n)}$

$$A_\ell^{(n)} \equiv \frac{\omega}{4\pi\sqrt{\pi(2\ell+1)}} \int_{\Omega} {}_2Y_{\ell,-2}(\theta, \phi) \overline{\mathcal{N}}_{++}^{(n)}(x, \phi), \quad (\text{IV.22})$$

$$B_\ell^{(n)} \equiv \frac{\omega}{4\pi\sqrt{\pi(2\ell+1)}} \int_{\Omega} {}_2Y_{\ell,-2}(\pi - \theta, \phi) \overline{\mathcal{N}}_{+-}^{(n)}(x, \phi).$$

The overline denotes the standard partial-wave regularisation of the leading helicity-preserving Coulomb pole. At the 4PM order, no new forward singularity is expected in the  $\mathcal{N}$ -matrix element.

The matching statement is that these two WQFT projections equal the two independent parity combinations of the BHPT phase shift [64]

$$\begin{aligned} A_\ell^{(n)} &= \sum_{P=\pm 1} -2\delta_{\ell 2}^{P,(n)}, \\ B_\ell^{(n)} &= (-1)^\ell \sum_{P=\pm 1} P -2\delta_{\ell 2}^{P,(n)}. \end{aligned} \quad (\text{IV.23})$$

At 4PM, we checked explicitly that Eq. (IV.23) is numerically satisfied up to  $\ell = 10$ , using publicly available codes for the computation of BHPT coefficients [124, 125].

## V. OUTLOOK

We have computed the minimal spinless gravitational Compton amplitude at fourth post-Minkowskian order using WQFT. This provides, to our knowledge, the first fully analytic three-loop determination of the classical spinless Compton amplitude in this setup. The calculation required the construction of the three-loop integrand, its reduction to 15 master integrals, and their subsequent evaluation. The master integrals were solved analytically using the method of canonical differential

equations, revealing the presence of an elliptic sector. After subtracting the lower-order Born iterations, we extracted the corresponding fourth-order  $N$ -matrix element and found agreement with the spinless BHPT phase shift.

Our result opens several directions. First, the integral basis, reduction strategy, and analytic methods developed here provide the natural starting point for including spin and spin-induced finite-size effects. Second, the same framework can be used to determine non-minimal worldline couplings, including tidal and absorptive response coefficients, by matching to black-hole perturbation theory at higher post-Minkowskian orders. Finally, the emergence of elliptic sectors already at three loops indicates that higher-order gravitational-wave scattering probes increasingly rich classes of special functions. The present computation therefore provides both a concrete fourth-order result and a template for extending amplitude-based methods to more general compact-object dynamics.

## ACKNOWLEDGMENTS

We are very grateful to the authors of [126] for sharing preliminary results for the  $T$ -matrix and for coordinating on submission. We wish to thank Stefano De Angelis, Gustav Jakobsen, Pierpaolo Mastrolia, and Lorenzo Tancredi for useful discussions.

We would like to further acknowledge Xiao Liu and Yan-Qing Ma for their invaluable help in the use of AM-FLOW. The computations for this work were performed with computing and storage resources provided by the CloudVeneto initiative at the University of Padova and INFN.

G.B.'s research is supported by the Italian MIUR under contract 20223ANFHR (PRIN2022), by the ERC (NOTIMEFORCOSMO, 101126304), and by the INFN initiatives *Amplitudes* and *TPPC*. S.S.'s research is partially supported by the INFN initiatives *Amplitudes*.

- 
- [1] T. Regge and J. A. Wheeler, *Phys. Rev.* **108**, 1063 (1957).
  - [2] F. J. Zerilli, *Phys. Rev. Lett.* **24**, 737 (1970).
  - [3] S. A. Teukolsky, *Astrophys. J.* **185**, 635 (1973).
  - [4] S. Mano, H. Suzuki, and E. Takasugi, *Prog. Theor. Phys.* **95**, 1079 (1996), arXiv:gr-qc/9603020.
  - [5] S. R. Dolan, *Phys. Rev. D* **76**, 084001 (2007), arXiv:0705.2880 [gr-qc].
  - [6] W. D. Goldberger and I. Z. Rothstein, *Phys. Rev. D* **73**, 104029 (2006), arXiv:hep-th/0409156.
  - [7] W. D. Goldberger and I. Z. Rothstein, *Phys. Rev. D* **73**, 104030 (2006), arXiv:hep-th/0511133.
  - [8] S. Foffa and R. Sturani, *Class. Quant. Grav.* **31**, 043001 (2014), arXiv:1309.3474 [gr-qc].
  - [9] S. Foffa, P. Mastrolia, R. Sturani, and C. Sturm, *Phys. Rev. D* **95**, 104009 (2017), arXiv:1612.00482 [gr-qc].
  - [10] S. Foffa and R. Sturani, *Phys. Rev. D* **100**, 024047 (2019), arXiv:1903.05113 [gr-qc].
  - [11] S. Foffa, R. A. Porto, I. Rothstein, and R. Sturani, *Phys. Rev. D* **100**, 024048 (2019), arXiv:1903.05118 [gr-qc].
  - [12] S. Foffa, P. Mastrolia, R. Sturani, C. Sturm, and W. J. Torres Bobadilla, *Phys. Rev. Lett.* **122**, 241605 (2019), arXiv:1902.10571 [gr-qc].
  - [13] R. A. Porto, M. M. Riva, and Z. Yang, *JHEP* **04**, 050 (2025), arXiv:2409.05860 [gr-qc].
  - [14] R. A. Porto and M. M. Riva, (2026), arXiv:2604.09545 [gr-qc].
  - [15] G. Brunello, M. K. Mandal, P. Mastrolia, R. Patil, M. Pegorin, J. Ronca, S. Smith, J. Steinhoff, and W. J. Torres Bobadilla, (2025), arXiv:2512.19498 [hep-th].
  - [16] G. Brunello, M. K. Mandal, P. Mastrolia, R. Patil, M. Pegorin, S. Smith, and J. Steinhoff, (2026), arXiv:2604.14134 [hep-th].
  - [17] C. Cheung, I. Z. Rothstein, and M. P. Solon, *Phys. Rev. Lett.* **121**, 251101 (2018), arXiv:1808.02489 [hep-th].

- [18] N. E. J. Bjerrum-Bohr, P. H. Damgaard, G. Festuccia, L. Planté, and P. Vanhove, *Phys. Rev. Lett.* **121**, 171601 (2018), arXiv:1806.04920 [hep-th].
- [19] Z. Bern, C. Cheung, R. Roiban, C.-H. Shen, M. P. Solon, and M. Zeng, *Phys. Rev. Lett.* **122**, 201603 (2019), arXiv:1901.04424 [hep-th].
- [20] Z. Bern, C. Cheung, R. Roiban, C.-H. Shen, M. P. Solon, and M. Zeng, *JHEP* **10**, 206 (2019), arXiv:1908.01493 [hep-th].
- [21] J. Parra-Martinez, M. S. Ruf, and M. Zeng, *JHEP* **11**, 023 (2020), arXiv:2005.04236 [hep-th].
- [22] C. Cheung and M. P. Solon, *JHEP* **06**, 144 (2020), arXiv:2003.08351 [hep-th].
- [23] P. Di Vecchia, C. Heissenberg, R. Russo, and G. Veneziano, *JHEP* **07**, 169 (2021), arXiv:2104.03256 [hep-th].
- [24] A. Brandhuber, G. Chen, G. Travaglini, and C. Wen, *JHEP* **10**, 118 (2021), arXiv:2108.04216 [hep-th].
- [25] G. Kälin, Z. Liu, and R. A. Porto, *Phys. Rev. Lett.* **125**, 261103 (2020), arXiv:2007.04977 [hep-th].
- [26] C. Dlapa, G. Kälin, Z. Liu, and R. A. Porto, *Phys. Lett. B* **831**, 137203 (2022), arXiv:2106.08276 [hep-th].
- [27] Z. Bern, J. Parra-Martinez, R. Roiban, M. S. Ruf, C.-H. Shen, M. P. Solon, and M. Zeng, *Phys. Rev. Lett.* **126**, 171601 (2021), arXiv:2101.07254 [hep-th].
- [28] Z. Bern, J. Parra-Martinez, R. Roiban, M. S. Ruf, C.-H. Shen, M. P. Solon, and M. Zeng, *PoS LL2022*, 051 (2022).
- [29] C. Dlapa, G. Kälin, Z. Liu, J. Neef, and R. A. Porto, *Phys. Rev. Lett.* **130**, 101401 (2023), arXiv:2210.05541 [hep-th].
- [30] G. U. Jakobsen, G. Mogull, J. Plefka, B. Sauer, and Y. Xu, *Phys. Rev. Lett.* **131**, 151401 (2023), arXiv:2306.01714 [hep-th].
- [31] G. U. Jakobsen, G. Mogull, J. Plefka, and B. Sauer, *Phys. Rev. Lett.* **131**, 241402 (2023), arXiv:2308.11514 [hep-th].
- [32] P. H. Damgaard, E. R. Hansen, L. Planté, and P. Vanhove, *JHEP* **09**, 183 (2023), arXiv:2307.04746 [hep-th].
- [33] Z. Bern, E. Herrmann, R. Roiban, M. S. Ruf, A. V. Smirnov, V. A. Smirnov, and M. Zeng, *Phys. Rev. Lett.* **132**, 251601 (2024), arXiv:2305.08981 [hep-th].
- [34] M. Driesse, G. U. Jakobsen, G. Mogull, J. Plefka, B. Sauer, and J. Usovitsch, *Phys. Rev. Lett.* **132**, 241402 (2024), arXiv:2403.07781 [hep-th].
- [35] Z. Bern, E. Herrmann, R. Roiban, M. S. Ruf, A. V. Smirnov, V. A. Smirnov, and M. Zeng, *JHEP* **10**, 023 (2024), arXiv:2406.01554 [hep-th].
- [36] M. Driesse, G. U. Jakobsen, A. Klemm, G. Mogull, C. Nega, J. Plefka, B. Sauer, and J. Usovitsch, *Nature* **641**, 603 (2025), arXiv:2411.11846 [hep-th].
- [37] Z. Bern, E. Herrmann, R. Roiban, M. S. Ruf, A. V. Smirnov, S. Smith, and M. Zeng, (2025), arXiv:2512.23654 [hep-th].
- [38] M. Driesse, G. U. Jakobsen, G. Mogull, C. Nega, J. Plefka, B. Sauer, and J. Usovitsch, (2026), arXiv:2601.16256 [hep-th].
- [39] C. Dlapa, G. Kälin, Z. Liu, and R. A. Porto, (2026), arXiv:2604.25916 [hep-th].
- [40] D. A. Kosower, B. Maybee, and D. O’Connell, *JHEP* **02**, 137 (2019), arXiv:1811.10950 [hep-th].
- [41] G. Mogull, J. Plefka, and J. Steinhoff, *JHEP* **02**, 048 (2021), arXiv:2010.02865 [hep-th].
- [42] G. U. Jakobsen, G. Mogull, J. Plefka, and J. Steinhoff, *Phys. Rev. Lett.* **126**, 201103 (2021), arXiv:2101.12688 [gr-qc].
- [43] G. Kälin and R. A. Porto, *JHEP* **11**, 106 (2020), arXiv:2006.01184 [hep-th].
- [44] G. Kälin, J. Neef, and R. A. Porto, *JHEP* **01**, 140 (2023), arXiv:2207.00580 [hep-th].
- [45] S. Mougiakakos, M. M. Riva, and F. Vernizzi, *Phys. Rev. D* **104**, 024041 (2021), arXiv:2102.08339 [gr-qc].
- [46] G. U. Jakobsen, G. Mogull, J. Plefka, and J. Steinhoff, *Phys. Rev. Lett.* **128**, 011101 (2022), arXiv:2106.10256 [hep-th].
- [47] S. De Angelis, P. P. Novichkov, and R. Gonzo, *Phys. Rev. D* **110**, L041502 (2024), arXiv:2309.17429 [hep-th].
- [48] A. Brandhuber, G. R. Brown, G. Chen, J. Gowdy, and G. Travaglini, *JHEP* **02**, 026 (2024), arXiv:2310.04405 [hep-th].
- [49] R. Aoude, K. Haddad, C. Heissenberg, and A. Helset, *Phys. Rev. D* **109**, 036007 (2024), arXiv:2310.05832 [hep-th].
- [50] A. Falkowski and P. Marinellis, *Eur. Phys. J. C* **85**, 74 (2025), arXiv:2407.16457 [hep-th].
- [51] G. Brunello, V. Chestnov, G. Crisanti, M. Giroux, and S. Smith, *Phys. Rev. D* **113**, 085011 (2026), arXiv:2510.26874 [hep-th].
- [52] A. Brandhuber, G. R. Brown, G. Chen, S. De Angelis, J. Gowdy, and G. Travaglini, *JHEP* **06**, 048 (2023), arXiv:2303.06111 [hep-th].
- [53] A. Herderschee, R. Roiban, and F. Teng, *JHEP* **06**, 004 (2023), arXiv:2303.06112 [hep-th].
- [54] A. Georgoudis, C. Heissenberg, and I. Vazquez-Holm, *JHEP* **06**, 126 (2023), arXiv:2303.07006 [hep-th].
- [55] A. Elkhidir, D. O’Connell, M. Sergola, and I. A. Vazquez-Holm, *JHEP* **07**, 272 (2024), arXiv:2303.06211 [hep-th].
- [56] S. Caron-Huot, M. Giroux, H. S. Hannesdottir, and S. Mizera, *JHEP* **01**, 139 (2024), arXiv:2308.02125 [hep-th].
- [57] L. Bohnenblust, H. Ita, M. Kraus, and J. Schlenk, *JHEP* **11**, 109 (2024), arXiv:2312.14859 [hep-th].
- [58] G. Brunello and S. De Angelis, *JHEP* **07**, 062 (2024), arXiv:2403.08009 [hep-th].
- [59] L. Bohnenblust, H. Ita, M. Kraus, and J. Schlenk, *JHEP* **12**, 100 (2025), arXiv:2505.15724 [hep-th].
- [60] G. Brunello, S. De Angelis, and D. A. Kosower, (2025), arXiv:2511.05412 [hep-th].
- [61] N. E. J. Bjerrum-Bohr, G. Chen, C. J. Eriksen, and N. Shah, *JHEP* **10**, 235 (2025), arXiv:2506.19705 [hep-th].
- [62] D. Akpinar, *Phys. Rev. D* **113**, 045003 (2026), arXiv:2511.10280 [hep-th].
- [63] N. E. J. Bjerrum-Bohr, G. Chen, C. Jordan Eriksen, and N. Shah, (2026), arXiv:2602.06947 [hep-th].
- [64] Y. F. Bautista, M. Driesse, K. Haddad, and G. U. Jakobsen, *JHEP* **05**, 252 (2026), arXiv:2602.06125 [hep-th].
- [65] M. M. Ivanov, Y.-Z. Li, J. Parra-Martinez, and Z. Zhou, (2026), arXiv:2602.06951 [hep-th].
- [66] P. H. Damgaard, L. Plante, and P. Vanhove, *JHEP* **11**, 213 (2021), arXiv:2107.12891 [hep-th].
- [67] P. Di Vecchia, C. Heissenberg, R. Russo, and G. Veneziano, *Phys. Rept.* **1083**, 1 (2024), arXiv:2306.16488 [hep-th].
- [68] J.-W. Kim, R. Patil, T. Scheopner, and J. Steinhoff, *JHEP* **03**, 241 (2026), arXiv:2511.05649 [hep-th].

- [69] M. M. Ivanov and Z. Zhou, *Phys. Rev. Lett.* **130**, 091403 (2023), [arXiv:2209.14324 \[hep-th\]](#).
- [70] M. V. S. Saketh, Z. Zhou, and M. M. Ivanov, *Phys. Rev. D* **109**, 064058 (2024), [arXiv:2307.10391 \[hep-th\]](#).
- [71] M. M. Ivanov, Y.-Z. Li, J. Parra-Martinez, and Z. Zhou, *Phys. Rev. Lett.* **132**, 131401 (2024), [Erratum: *Phys.Rev.Lett.* 134, 159901 (2025)], [arXiv:2401.08752 \[hep-th\]](#).
- [72] S. Caron-Huot, M. Correia, G. Isabella, and M. Solon, *Phys. Rev. Lett.* **135**, 191601 (2025), [arXiv:2503.13593 \[hep-th\]](#).
- [73] F. V. Tkachov, *Phys. Lett. B* **100**, 65 (1981).
- [74] K. G. Chetyrkin and F. V. Tkachov, *Nucl. Phys. B* **192**, 159 (1981).
- [75] S. Laporta, *Int. J. Mod. Phys. A* **15**, 5087 (2000), [arXiv:hep-ph/0102033](#).
- [76] A. V. Kotikov, *Phys. Lett. B* **254**, 158 (1991).
- [77] A. V. Kotikov, *Phys. Lett. B* **267**, 123 (1991), [Erratum: *Phys.Lett.B* 295, 409–409 (1992)].
- [78] E. Remiddi, *Nuovo Cim. A* **110**, 1435 (1997), [arXiv:hep-th/9711188](#).
- [79] T. Gehrmann and E. Remiddi, *Nucl. Phys. B* **580**, 485 (2000), [arXiv:hep-ph/9912329](#).
- [80] M. Argeri and P. Mastrolia, *Int. J. Mod. Phys. A* **22**, 4375 (2007), [arXiv:0707.4037 \[hep-ph\]](#).
- [81] J. M. Henn, *Phys. Rev. Lett.* **110**, 251601 (2013), [arXiv:1304.1806 \[hep-th\]](#).
- [82] M. Argeri, S. Di Vita, P. Mastrolia, E. Mirabella, J. Schlenk, U. Schubert, and L. Tancredi, *JHEP* **03**, 082 (2014), [arXiv:1401.2979 \[hep-ph\]](#).
- [83] J. S. Schwinger, *J. Math. Phys.* **2**, 407 (1961).
- [84] L. V. Keldysh, *Sov. Phys. JETP* **30**, 1018 (1965).
- [85] G. U. Jakobsen, G. Mogull, J. Plefka, and B. Sauer, *JHEP* **10**, 128 (2022), [arXiv:2207.00569 \[hep-th\]](#).
- [86] F. A. Berends and W. T. Giele, *Nucl. Phys. B* **306**, 759 (1988).
- [87] G. U. Jakobsen, *Gravitational Scattering of Compact Bodies from Worldline Quantum Field Theory*, Ph.D. thesis, Humboldt U., Berlin, Humboldt U., Berlin (main) (2023), [arXiv:2308.04388 \[hep-th\]](#).
- [88] J. Davies, T. Kaneko, C. Marinissen, T. Ueda, and J. A. M. Vermaseren, (2026), [arXiv:2601.19982 \[hep-ph\]](#).
- [89] C. Anastasiou, J. Karlen, and M. Vicini, *JHEP* **12**, 169 (2023), [arXiv:2308.14701 \[hep-ph\]](#).
- [90] G. Brunello, P. Mastrolia, J. Ronca, S. Smith, and M. Zeng, in progress.
- [91] J. Gluza, K. Kajda, and D. A. Kosower, *Phys. Rev. D* **83**, 045012 (2011), [arXiv:1009.0472 \[hep-th\]](#).
- [92] Z. Wu, J. Boehm, R. Ma, H. Xu, and Y. Zhang, *Comput. Phys. Commun.* **295**, 108999 (2024), [arXiv:2305.08783 \[hep-ph\]](#).
- [93] Z. Wu, J. Böhm, R. Ma, J. Usovitsch, Y. Xu, and Y. Zhang, *Comput. Phys. Commun.* **316**, 109798 (2025), [arXiv:2502.20778 \[hep-ph\]](#).
- [94] S. Smith and M. Zeng, (2025), [arXiv:2507.11140 \[hep-th\]](#).
- [95] F. Lange, J. Usovitsch, and Z. Wu, (2025), [arXiv:2505.20197 \[hep-ph\]](#).
- [96] T. Peraro, *JHEP* **07**, 031 (2019), [arXiv:1905.08019 \[hep-ph\]](#).
- [97] W. Flieger and W. J. Torres Bobadilla, *Eur. Phys. J. Plus* **139**, 1022 (2024), [arXiv:2210.09872 \[hep-th\]](#).
- [98] L. Görge, C. Nega, L. Tancredi, and F. J. Wagner, *JHEP* **07**, 206 (2023), [arXiv:2305.14090 \[hep-th\]](#).
- [99] C. Duhr, S. Maggio, C. Nega, B. Sauer, L. Tancredi, and F. J. Wagner, *JHEP* **06**, 128 (2025), [arXiv:2503.20655 \[hep-th\]](#).
- [100] F. Forner, C. C. Mella, C. Nega, L. Tancredi, and F. J. Wagner, (2026), [arXiv:2604.25270 \[hep-th\]](#).
- [101] C. Meyer, *Comput. Phys. Commun.* **222**, 295 (2018), [arXiv:1705.06252 \[hep-ph\]](#).
- [102] K.-T. Chen, *Bull. Am. Math. Soc.* **83**, 831 (1977).
- [103] E. Remiddi and J. A. M. Vermaseren, *Int. J. Mod. Phys. A* **15**, 725 (2000), [arXiv:hep-ph/9905237](#).
- [104] J. Broedel, C. Duhr, F. Dulat, B. Penante, and L. Tancredi, *JHEP* **01**, 023 (2019), [arXiv:1809.10698 \[hep-th\]](#).
- [105] C. Duhr and F. Dulat, *JHEP* **08**, 135 (2019), [arXiv:1904.07279 \[hep-th\]](#).
- [106] M. Beneke and V. A. Smirnov, *Nucl. Phys. B* **522**, 321 (1998), [arXiv:hep-ph/9711391](#).
- [107] A. Pak and A. Smirnov, *Eur. Phys. J. C* **71**, 1626 (2011), [arXiv:1011.4863 \[hep-ph\]](#).
- [108] B. Jantzen, A. V. Smirnov, and V. A. Smirnov, *Eur. Phys. J. C* **72**, 2139 (2012), [arXiv:1206.0546 \[hep-ph\]](#).
- [109] P. Mastrolia, M. Passera, A. Primo, and U. Schubert, *JHEP* **11**, 198 (2017), [arXiv:1709.07435 \[hep-ph\]](#).
- [110] F. Dulat and B. Mistlberger, (2014), [arXiv:1411.3586 \[hep-ph\]](#).
- [111] V. Chestnov, S. J. Matsubara-Heo, H. J. Munch, and N. Takayama, *JHEP* **11**, 202 (2023), [arXiv:2305.01585 \[hep-th\]](#).
- [112] S. Laporta, *Phys. Lett. B* **523**, 95 (2001), [arXiv:hep-ph/0111123](#).
- [113] R. N. Lee and V. A. Smirnov, *JHEP* **02**, 102 (2011), [arXiv:1010.1334 \[hep-ph\]](#).
- [114] K. G. Chetyrkin and A. G. Grozin, *Nucl. Phys. B* **666**, 289 (2003), [arXiv:hep-ph/0303113](#).
- [115] C. Dlapa, G. Kälin, Z. Liu, and R. A. Porto, *JHEP* **08**, 109 (2023), [arXiv:2304.01275 \[hep-th\]](#).
- [116] R. Jinno, G. Kälin, Z. Liu, and H. Rubira, *JHEP* **07**, 181 (2023), [arXiv:2209.01091 \[hep-th\]](#).
- [117] X. Liu and Y.-Q. Ma, *Comput. Phys. Commun.* **283**, 108565 (2023), [arXiv:2201.11669 \[hep-ph\]](#).
- [118] S. Weinberg, *Phys. Rev.* **140**, B516 (1965).
- [119] S. Weinberg, *The Quantum theory of fields. Vol. 1: Foundations* (Cambridge University Press, 2005).
- [120] S. Weinberg, *The quantum theory of fields. Vol. 2: Modern applications* (Cambridge University Press, 2013).
- [121] A. Brandhuber, G. R. Brown, P. Pichini, G. Travaglini, and P. Vives Matasan, (2025), [arXiv:2512.05017 \[hep-th\]](#).
- [122] C. Anastasiou and K. Melnikov, *Nucl. Phys. B* **646**, 220 (2002), [arXiv:hep-ph/0207004](#).
- [123] C. Anastasiou, K. Melnikov, and F. Petriello, *Phys. Rev. D* **69**, 076010 (2004), [arXiv:hep-ph/0311311](#).
- [124] “Black Hole Perturbation Toolkit,” <https://bhptoolkit.org>.
- [125] J. Markovic and M. M. Ivanov, (2025), [arXiv:2511.04765 \[gr-qc\]](#).
- [126] Y. F. Bautista, M. Driesse, K. Haddad, and G. U. Jakobsen, To appear.
- [127] V. A. Smirnov, *Analytic tools for Feynman integrals*, Vol. 250 (2012).



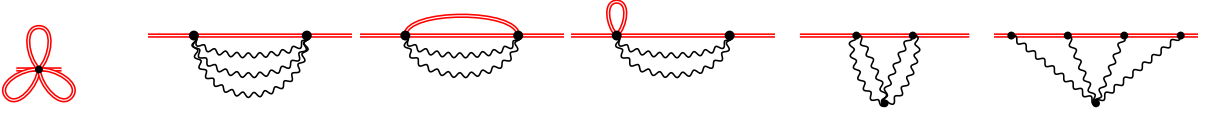


FIG. 7. 6 master integrals of the hard boundary region.

a. *Hard region.* The first five boundary master integrals in the hard region, Eq. (III.30), read as:

$$F_{111000000}^{\text{h}}(\eta_1, \eta_2, \eta_3) = \mu^{6\epsilon} e^{3\epsilon\gamma_E} \omega^{3-6\epsilon} \left[ \frac{e^{i\pi(\eta_1+\eta_2+\eta_3)(\epsilon-\frac{1}{2})}}{(4\pi)^{\frac{9}{2}}} \Gamma^3\left(\epsilon - \frac{1}{2}\right) \right], \quad (\text{B.1})$$

$$F_{100001110}^{\text{h}}(\eta_1, \eta_2, \eta_3) = \mu^{6\epsilon} e^{3\epsilon\gamma_E} \omega^{1-6\epsilon} \left[ \frac{e^{i\pi\eta_1(3\epsilon-\frac{1}{2})}}{(4\pi)^{\frac{9}{2}}} \frac{\Gamma^3\left(\frac{1}{2}-\epsilon\right) \Gamma(2\epsilon) \Gamma(3\epsilon-\frac{1}{2}) \Gamma(2-6\epsilon)}{\Gamma\left(\frac{3}{2}-3\epsilon\right) \Gamma(2-4\epsilon)} \right], \quad (\text{B.2})$$

$$F_{101000110}^{\text{h}}(\eta_1, \eta_2, \eta_3) = \mu^{6\epsilon} e^{3\epsilon\gamma_E} \omega^{1-6\epsilon} \frac{\Gamma^2\left(\frac{1}{2}-\epsilon\right) \Gamma^2(2\epsilon) \Gamma\left(\epsilon+\frac{1}{2}\right) \Gamma\left(3\epsilon-\frac{1}{2}\right)}{(4\pi)^{\frac{9}{2}} \Gamma(4\epsilon) \Gamma\left(\frac{3}{2}-\epsilon\right)} \left[ e^{i\pi\eta_3(3\epsilon-\frac{1}{2})} \left( \frac{1+\eta_1\eta_3}{2} \right) + \frac{\sin \pi\epsilon}{\cos 2\pi\epsilon} \left( \frac{1-\eta_1\eta_3}{2} \right) \right], \quad (\text{B.3})$$

$$F_{110001010}^{\text{h}}(\eta_1, \eta_2, \eta_3) = \mu^{6\epsilon} e^{3\epsilon\gamma_E} \omega^{1-6\epsilon} \left[ \frac{e^{i\pi[2\epsilon\eta_2-\eta_1(\frac{1}{2}-\epsilon)]}}{(4\pi)^{\frac{9}{2}}} \frac{\Gamma^2\left(\frac{1}{2}-\epsilon\right) \Gamma\left(\frac{1}{2}+\epsilon\right) \Gamma(2\epsilon) \Gamma(1-4\epsilon) \Gamma\left(\epsilon-\frac{1}{2}\right)}{\Gamma(1-2\epsilon) \Gamma\left(\frac{3}{2}-3\epsilon\right)} \right], \quad (\text{B.4})$$

$$F_{010101110}^{\text{h}}(\eta_1, \eta_2, \eta_3) = \mu^{6\epsilon} e^{3\epsilon\gamma_E} \omega^{-1-6\epsilon} \left[ \frac{e^{i\pi\eta_2(\frac{1}{2}+3\epsilon)}}{(4\pi)^{\frac{9}{2}}} \frac{\Gamma^2\left(\frac{1}{2}+\epsilon\right) \Gamma^4\left(\frac{1}{2}-\epsilon\right) \Gamma\left(\frac{1}{2}+3\epsilon\right) \Gamma(-6\epsilon)}{\Gamma^2(1-2\epsilon) \Gamma(1-4\epsilon)} \right]. \quad (\text{B.5})$$

Such expressions were derived using a combination of methods: integrals 1,2,4, and 5 were computed by recursively applying formulas for massless bubble and tadpole integrals, while integral 3 was obtained via Mellin–Barnes techniques. Integral 6 was obtained by reconstructing the numerical result obtained up to  $O(\epsilon^2)$  using AMFLOW, for retarded propagators and for the various cut configurations, giving:

$$F_{111101110}^{\text{h}(+++)} = i\mu^{6\epsilon} \omega^{-5-6\epsilon} \frac{e^{3i\epsilon\pi}}{(16\pi)^3} \left[ \frac{1}{3\epsilon^2} - \frac{7+6\log(2)}{3\epsilon} + 15 + 14\log(2) + \frac{29\pi^2}{36} + 6\log^2(2) \right. \\ \left. + \left( 31\zeta(3) - 93 - \frac{1}{12}\pi^2(57+58\log(2)) - 6\log(2)(15+\log(2)(7+2\log(2))) \right) \epsilon + \mathcal{O}(\epsilon^2) \right], \quad (\text{B.6})$$

$$F_{111101110}^{\text{h}(ccc)} = -\frac{\mu^{6\epsilon} \omega^{-5-6\epsilon}}{(16\pi)^3} \left[ \frac{4}{3\epsilon^2} - \frac{1}{\epsilon} \left( \frac{44}{3} + 8\log 2 \right) + \left( \frac{316}{3} + 88\log 2 + 24\log^2 2 - \frac{241\pi^2}{9} \right) \right. \\ \left. + \epsilon \left( -\frac{6092}{9} - 632\log 2 - 264\log^2 2 - 48\log^3 2 + \frac{\pi^2}{9} (2203 + 1446\log 2) + 124\zeta_3 \right) \right] + \mathcal{O}(\epsilon^2), \quad (\text{B.7})$$

$$F_{111101110}^{\text{h}(cc+)} = -\frac{i\mu^{6\epsilon} \omega^{-5-6\epsilon}}{(16\pi)^3} \left[ -\frac{2}{3\epsilon^2} + \frac{2}{3\epsilon} (11 + i\pi + 6\log 2) + \frac{1}{18} [241\pi^2 - 12(79 + 66\log 2 + 18\log^2 2) - 12i\pi(5 + 6\log 2)] \right] \\ + \frac{\epsilon}{18} [4(1523 + 1422\log 2 + 594\log^2 2 + 108\log^3 2 - 279\zeta_3) - \pi^2(2203 + 1446\log 2) \\ + i\pi(3\pi^2 + 36(9 + 10\log 2 + 6\log^2 2))] + \mathcal{O}(\epsilon^2), \quad (\text{B.8})$$

$$F_{111101110}^{\text{h}(c+c)} = -\frac{i\mu^{6\epsilon} \omega^{-5-6\epsilon}}{(16\pi)^3} \left[ -\frac{2}{3\epsilon^2} + \frac{2}{3\epsilon} (11 - 5i\pi + 6\log 2) + \frac{1}{18} [241\pi^2 + 2i\pi(407 + 180\log 2) - 12(79 + 66\log 2 + 18\log^2 2)] \right] \\ + \frac{\epsilon}{18} [4(1523 + 1422\log 2 + 594\log^2 2 + 108\log^3 2 - 279\zeta_3) - \pi^2(2203 + 1446\log 2) \\ + i\pi(513\pi^2 - 12(319 + 282\log 2 + 90\log^2 2))] + \mathcal{O}(\epsilon^2), \quad (\text{B.9})$$

$$F_{111101110}^{\text{h}(+cc)} = F_{111101110}^{\text{h}(cc+)}. \quad (\text{B.10})$$



FIG. 8. 6 master integrals of the soft boundary region.

*b. Soft region.* The boundary master integrals in the soft region, Eq. (III.33), read as:

$$F_{0001000011110}^S(\eta_1 \eta_2 \eta_3) = \mu^{6\epsilon} e^{3\epsilon\gamma_E} \omega^{1-6\epsilon} \left[ \frac{1}{(4\pi)^{\frac{9}{2}}} \frac{\Gamma^4\left(\frac{1}{2} - \epsilon\right) \Gamma\left(3\epsilon - \frac{1}{2}\right)}{2^{6\epsilon-1} \Gamma(2-4\epsilon)} \right], \quad (\text{B.11})$$

$$F_{0011000011110}^S(\eta_1 \eta_2 \eta_3) = \mu^{6\epsilon} e^{3\epsilon\gamma_E} \omega^{-1-6\epsilon} \left[ \frac{e^{\frac{i\pi}{2}\eta_3} \sqrt{\pi} \Gamma^3\left(\frac{1}{2} - \epsilon\right) \Gamma(-\epsilon) \Gamma(1-3\epsilon) \Gamma(3\epsilon)}{(4\pi)^{\frac{9}{2}}} \frac{2^{6\epsilon} \Gamma\left(\frac{3}{2} - 3\epsilon\right) \Gamma(1-4\epsilon)}{\Gamma(1-4\epsilon)} \right], \quad (\text{B.12})$$

$$F_{0101000011110}^S(\eta_1 \eta_2 \eta_3) = \mu^{6\epsilon} e^{3\epsilon\gamma_E} \omega^{-1-6\epsilon} \left[ \frac{e^{\frac{i\pi}{2}\eta_2} \sqrt{\pi} \Gamma^4\left(\frac{1}{2} - \epsilon\right) \Gamma^2\left(\frac{1}{2} - 2\epsilon\right) \Gamma(3\epsilon)}{(4\pi)^{\frac{9}{2}}} \frac{2^{6\epsilon} \Gamma^2(1-2\epsilon) \Gamma(1-4\epsilon)}{\Gamma(1-4\epsilon)} \right], \quad (\text{B.13})$$

$$F_{0111000011110}^S(\eta_1 \eta_2 \eta_3) = \mu^{6\epsilon} e^{3\epsilon\gamma_E} \omega^{-3-6\epsilon} \left\{ \frac{\eta_2 \eta_3}{(4\pi)^{\frac{9}{2}}} \frac{\Gamma^2\left(\frac{1}{2} - \epsilon\right)}{2^{6\epsilon+1} \Gamma(1-2\epsilon)} \left[ -\frac{\pi \Gamma\left(\frac{1}{2} - 2\epsilon\right) \Gamma^2(-\epsilon) \Gamma\left(\frac{1}{2} + 3\epsilon\right)}{\Gamma\left(\frac{1}{2} - 4\epsilon\right)} - \eta_2 \eta_3 \Gamma\left(\frac{3}{2} - \epsilon\right) \Gamma\left(-\frac{1}{2} + \epsilon\right) \times \right. \right. \\ \left. \times \left( \Gamma\left(\frac{5}{2} - 3\epsilon\right) \Gamma(-2\epsilon) \Gamma(-\epsilon) \Gamma\left(-\frac{3}{2} + 3\epsilon\right) {}_3\tilde{F}_2\left(\begin{matrix} -\epsilon, -2\epsilon, \frac{1}{2} - 3\epsilon \\ 1 - \epsilon, \frac{1}{2} - 5\epsilon \end{matrix}; 1 \right) \right. \right. \\ \left. \left. - \sqrt{\pi} \Gamma(1-2\epsilon) \Gamma\left(\frac{1}{2} - \epsilon\right) \Gamma\left(\frac{1}{2} + 3\epsilon\right) {}_4\tilde{F}_3\left(\begin{matrix} \frac{1}{2}, 1, \frac{1}{2} - \epsilon, 1 - 2\epsilon \\ \frac{3}{2}, \frac{3}{2} + \epsilon, 1 - 4\epsilon \end{matrix}; 1 \right) \right] \right\}, \quad (\text{B.14})$$

$$F_{1011000011110}^S(\eta_1 \eta_2 \eta_3) = \mu^{6\epsilon} e^{3\epsilon\gamma_E} \omega^{-3-6\epsilon} \left\{ \frac{\eta_1 \eta_3}{(4\pi)^{\frac{9}{2}}} \frac{\Gamma^2\left(\frac{1}{2} - \epsilon\right)}{2^{6\epsilon+1} \Gamma(1-2\epsilon)} \left[ -\frac{\pi \Gamma\left(\frac{1}{2} - 2\epsilon\right) \Gamma^2(-\epsilon) \Gamma\left(\frac{1}{2} + 3\epsilon\right)}{\Gamma\left(\frac{1}{2} - 4\epsilon\right)} + \eta_1 \eta_3 \Gamma(1-2\epsilon) \Gamma(2\epsilon) \Gamma\left(\frac{1}{2} + 3\epsilon\right) \times \right. \right. \\ \left. \times \left( \Gamma^2\left(\frac{1}{2} - 3\epsilon\right) \Gamma\left(\frac{1}{2} - 2\epsilon\right) {}_3\tilde{F}_2\left(\begin{matrix} \frac{1}{2} - 2\epsilon, \frac{1}{2} - 3\epsilon, \frac{1}{2} - 3\epsilon \\ 1 - 6\epsilon, \frac{3}{2} - 2\epsilon \end{matrix}; 1 \right) \right. \right. \\ \left. \left. - \sqrt{\pi} \Gamma^2\left(\frac{1}{2} - \epsilon\right) {}_4\tilde{F}_3\left(\begin{matrix} \frac{1}{2}, 1, \frac{1}{2} - \epsilon, \frac{1}{2} - \epsilon \\ \frac{3}{2}, 1 - 4\epsilon, 1 + 2\epsilon \end{matrix}; 1 \right) \right] \right\}, \quad (\text{B.15})$$

$$F_{1111000011110}^S(\eta_1 \eta_2 \eta_3) = \mu^{6\epsilon} e^{3\epsilon\gamma_E} \omega^{-5-6\epsilon} \left( \frac{\eta_1 + \eta_3}{3} - \eta_1 \eta_2 \eta_3 \right) \left[ \frac{1}{(4\pi)^{\frac{9}{2}}} \frac{i \pi^{3/2} \Gamma^4(-\epsilon) \Gamma(3\epsilon + 1)}{2^{6\epsilon+2} \Gamma(-4\epsilon)} \right], \quad (\text{B.16})$$

where we used

$${}_p\tilde{F}_q(\vec{a}; \vec{b}; z) = \frac{{}_pF_q(\vec{a}; \vec{b}; z)}{\Gamma(b_1) \cdots \Gamma(b_q)}. \quad (\text{B.17})$$

The first three integrals are derived analytically using standard massless bubble and tadpole integrals together with the result of [115, 127]

$$\int_{\mathcal{L}} \frac{1}{[\pm \ell \cdot \mathbf{n} - i0^+]^{\alpha_1} [\ell^2]^{\beta_1} [(\ell - \hat{\mathbf{q}})^2]^{\beta_2}} = \frac{e^{\epsilon\gamma_E} 2^{\alpha_1-1} i^{\alpha_1} \Gamma\left(\frac{\alpha_1}{2}\right) \Gamma\left(\frac{d-\alpha_1}{2} - \beta_1\right) \Gamma\left(\frac{d-\alpha_1}{2} - \beta_2\right) \Gamma\left(\frac{\alpha_1-d}{2} + \beta_1 + \beta_2\right)}{(4\pi)^{\frac{3}{2}} \Gamma(\alpha_1) \Gamma(\beta_1) \Gamma(\beta_2) \Gamma(d - \alpha_1 - \beta_1 - \beta_2)}, \quad (\text{B.18})$$

where  $d = D - 1$ ,  $\beta_1 > 0$ ,  $\beta_2 > 0$ ,  $\mathbf{n} \cdot \hat{\mathbf{q}} = 0$ , and  $\hat{\mathbf{q}}^2 = 1$ . These derivations were generalized to arbitrary prescriptions. The fourth and fifth integrals require a dedicated derivation based on a combination of Schwinger and Feynman parameterizations. The full derivation of these integrals can be found in Refs. [115, 116], together with the computation of the sixth top-sector integral. These results have been verified numerically using AMFlow.